High-diodicity impinging injector design for rocket propulsion enabled by additive manufacturing

Alex R Keller, Joel Otomize, Anil P Nair, Nicolas Q Minesi, R Mitchell Spearrin

High-diodicity impinging injector design for rocket propulsion enabled by additive manufacturing

Alex R. Keller*, Joel Otomize†, Anil P. Nair‡, Nicolas Q. Minesi§, and R. Mitchell Spearrin¶
University of California, Los Angeles (UCLA), Los Angeles, CA, 90095

This work examines novel impinging injector designs enabled by additive manufacturing that reduce forward pressure loss while maintaining high relative back-flow resistance (diodicity). A steady, non-reacting computational fluid dynamics (CFD) model is used to assess the hydraulic characteristics of fluidic diode features in a liquid bi-propellant impinging doublet-type injector configuration relevant to rocket propulsion applications. A design trade study is conducted to determine an effective fluidic diode feature to be implemented within the injector elements, constrained by practical considerations for additive manufacturing. Noteworthy increases in diodicity are achieved within the constraints of producibility relative to conventional designs. A complimentary transient, multiphase CFD model is used to evaluate propellant backflow behavior when subject to a high-pressure impulse within a downstream chamber. Preliminary results suggest that the diodicity is a relevant predictor of transient performance as injector stiffness decreases.

I. Nomenclature

A	=	cross-sectional flow area
AM	=	additive manufacturing
C_D	=	discharge coefficient
CFD	=	computational fluid dynamics
Di	=	diodicity
EDM	=	electrical discharge machining
fu	=	fuel
fwd	=	forward flow
IS	=	injector stiffness
LPBF	=	laser powder bed fusion
$\dot{m}$	=	mass flow rate
NDE	=	nondestructive evaluation
ox	=	oxidizer
p_c	=	chamber pressure
Δp	=	pressure drop
p_in	=	inlet pressure
p_out	=	inlet pressure
R	=	diode radius
RDRE	=	rotating detonation rocket engine
rev	=	reverse flow
ρ	=	density

*Ph.D. Student, Department of Mechanical and Aerospace Engineering.
†Masters Student, Department of Mechanical and Aerospace Engineering.
‡Ph.D. Candidate, Department of Mechanical and Aerospace Engineering.
§Postdoctoral Scholar, Mechanical and Aerospace Engineering Department
¶Associate Professor, Department of Mechanical and Aerospace Engineering.

II. Introduction

Combustion instabilities are common in liquid rocket engines and present concerns for system performance and hardware survivability. Such instabilities often present as periodic, high-pressure impulses within a combustor that can negatively influence the fluid dynamics of the propellant injection process - in some cases leading to backflow of combustion products into the propellant manifolds. Backflow caused by combustion instabilities or from detonations within a combustor induces a decline in combustion efficiency due to poor mixing from discrepancies in characteristic recovery times between the fuel and oxidizer lines due to differences in orifice geometry, propellant densities, and inlet pressures. Specific injector designs have a characteristic resistance to feed system coupling and recovery time (related to backflow) that depends on injector geometry and stiffness (the ratio of the pressure drop across the injector to the pressure in the combustion chamber) [1]. For traditional combustion-based rocket engines, the injector stiffness is typically ~15-20% in order to mitigate the performance-reducing effects of combustion instabilities [1]. Increased injector stiffness requires larger (heavier) feed pressurization systems, leading to an increase in the dry mass of the overall vehicle, and results in a decreased payload or mission duration capability for spacecraft and launch vehicles.

An ongoing goal in improving rocket engine performance is the development of low pressure-loss injectors which are also robust against combustion instabilities and the associated feed-system coupling. An approach which allows for the simultaneous fulfillment of these requirements is the implementation of an injector geometry to resist reverse flow without hindering forward flow. Some recent efforts have explored geometric modifications to impinging injector schemes to enhance backflow resistance and recovery characteristics by angling injector elements relative to the direction of a transverse pressure/shock wave [2]. This angling resulted in only minimal performance improvements due to difficulty in predicting the direction of the wave propagation and a rise in potentially harmful cavitation near the injection plane. The tapering of injector orifices led to noticeably faster propellant recovery times, which is speculated to be the result of the product gases having a larger volume to fill and expand, thus decreasing its pressure [2]. In this work, we examine the potential of additive manufacturing to enable impinging injection designs that provide enhanced backflow resistance or diodicity.

Aside from the production-rate and possible economic benefits, additive manufacturing (AM) provides opportunity to re-imagine combustion device design in the absence of conventional manufacturing constraints, and to more closely couple design with physics-based analysis. AM enables complex three-dimensional geometries and provides a new means for tailoring the fluid dynamics of combustion systems, particularly injection. For example, AM permits the fabrication of bio-inspired propellant passageways within an injector's manifold, which encourage gradual changes in both flow area and direction. These geometric alterations in the flow paths mitigate flow separation and minimize viscous losses, ultimately decreasing the forward pressure drop across the injector [3]. In this work, the design space permitted by additive manufacturing is explored to create low forward pressure-loss impinging injection schemes that hinder propellant backflow. We investigate the implementation of a "fluidic diode" feature as a means of backflow prevention for a representative liquid bi-propellant impinging doublet. Steady single-phase and transient multi-phase CFD models are utilized to quantify backflow resistance and assess forward-flow recovery, respectively. Initial cold-flow results for select printed injectors are also presented, with a discussion of relative performance and future work.

III. Methods

A. Diodicity

Design efforts are driven by computational fluid dynamics analysis, and quantitatively characterized through calculating injector discharge coefficient, C_{D}, a key metric used to assess hydraulic performance, defined as:

$$C_D = \frac{\dot{m}}{A\sqrt{2\rho\Delta p}} \tag{1}$$

Here, $\dot{m}$ represents the mass flow rate of propellant with density ρ through an orifice with a cross-sectional flow area A, and a pressure drop Δp across the orifice.

Additionally, we calculate the diodicity of each injector as a means of characterizing its relative backflow resistance. Diodicity, Di, is defined in Eq. 2 as the ratio of pressure drop for reverse flow to the required pressure drop in forward flow for the same mass flow rate. This can be modeled by flipping the inlet and outlet boundary conditions in the CFD model, and calculating the discharge coefficient in the reverse direction. Diodicity can also be described in terms of

forward and reverse discharge coefficients, as also seen in Eq. 2:

$$\mathrm{Di} = \left(\frac{\Delta p_{\mathrm{rev}}}{\Delta p_{\mathrm{fwd}}}\right)_{\dot{m}} = \left(\frac{C_{D,\mathrm{fwd}}}{C_{D,\mathrm{rev}}}\right)^2 \tag{2}$$

B. Design of a fluidic diode

Here we introduce an AM-enabled, backflow-resistant flow-path geometry termed a "fluidic diode" [4]. Analogous to an electrical diode, which allows electric current to flow in a single forward direction while impeding flow in the opposite direction, this fluidic diode feature serves as a means of resisting the backflow of combustion gases up into the propellant manifold. Implemented slightly upstream of the propellant injector face, this feature is intended to perform similar to a Tesla valve [5] in which the geometry of the flow path provides for low resistance in the forward direction but induces high resistance in the reverse direction (see Fig. 1).

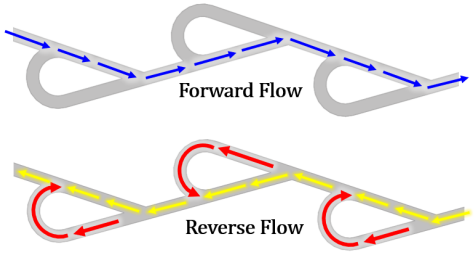

Fig. 1 Tesla valve flow behavior with low-resistance in forward direction (top) and high-resistance in reverse direction (bottom).

The flow path geometry of a Tesla valve promotes flow losses in the reverse direction from abrupt momentum changes, vorticity generation, and an adverse pressure gradient [6]. The fluidic diode developed in this work will combine the hydraulic benefits of "tapering" the injector element, demonstrated to be efficient in Ref. [2, 7], and the redirection of flow in the reverse direction similar to a Tesla valve.

Implementing these proposed diode features in a real rocket injector using conventional subtractive manufacturing techniques is impractical and thus leverages the unique capability of AM. However, the fluidic diode design is still constrained by two primary factors: 1) metal AM printability considerations such as sub-mm feature resolution and overhang angles [8] and 2) structural integrity of the injector. For example, the implementation of a fluidic diode cavity near the injection face can cause reductions in minimum wall-thickness between the unlike-doublet flow paths, and between adjacent doublet pairs. Furthermore, printed materials show a reduction in strength when sample thickness is below some characteristic value (dependent on material and AM fabrication process) due to increased porosity [9]. Therefore, the size, shape, and position of the fluidic diode must be taken into consideration throughout the design process.

A coupled CFD-design trade study was performed to examine how various fluidic diode geometries influence net diodicity. Parameters such as diode size, revolution angle, and number of diodes in series were examined (see Fig. 2). Orifice outlet diameter was held constant. A secondary design step involved integration of the various designs in the impinging doublet configuration with a 60 degree impingement angle, see Fig. 3. Based on relative diodicity results from steady-state simulations and feasibility assessment for manufacturing and structural integrity, a down-selected fluidic diode design was further analyzed with regards to transient response and compared to tapered impingement design without the diode feature. The analysis framework is discussed in the following subsections.

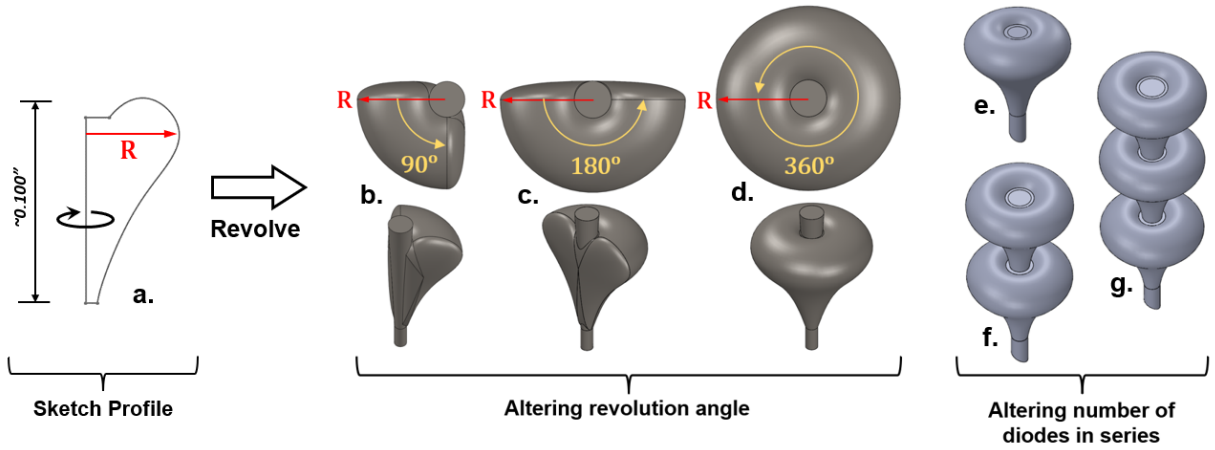

Fig. 2 a.) 2D sketch profile used to create a diode feature then revolved around at some desired angle. Top and isometric views of diode revolution angles of b.) 90°, c.) 180°, d.) 360°. The variation in the number of diodes in series is shown for e.) one, f.) two, and g.) three diodes.

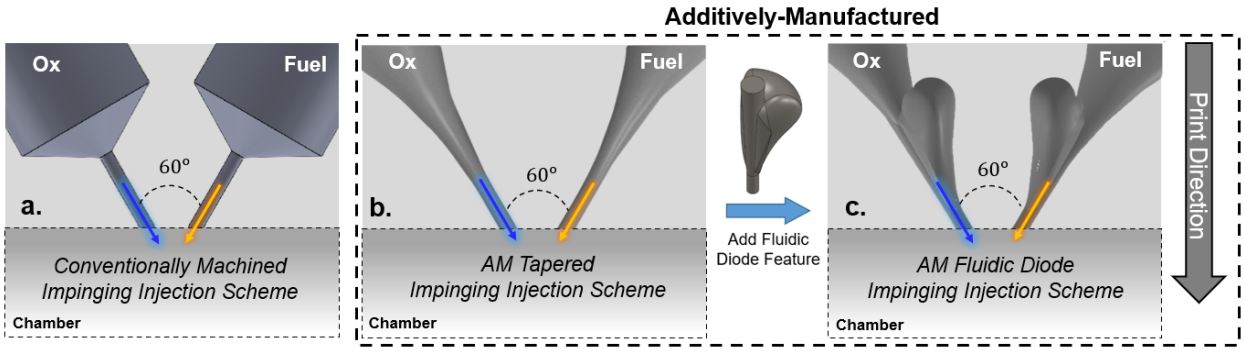

Fig. 3 Cross-sections of a.) conventional impinging injection scheme using subtractive manufacturing, b.) AM-enabled tapered impinging injection scheme, c.) the same tapered injection scheme as b. but with an example of implemented 90° fluidic diode of radius R = 0.050 in.

C. Steady-state CFD model

Discharge coefficients and diodicities are determined using steady, single-phase, three-dimensional computational fluid dynamics (CFD) analysis performed on the fluid domain of a single injection element for various impinging-doublet designs. Due to the injector's radial symmetry, a wedge-shaped slice of the injector's fluid domain was utilized. Unstructured, tetrahedral meshes of ~5×10^5 elements were used (see Fig. 4) following a brief mesh study where additional mesh sizes were examined to investigate the dependence of the results on mesh resolution. A no-slip boundary condition was applied to the injector walls, which also assume no surface roughness. An SST-k-ω turbulence model was applied and liquid water was used as the working fluid. The feed pressure was set to 300 psig at the inlet, and 0 psig at the outlet for forward flow. The pressure boundary conditions were then flipped to assess reverse-flow behavior. Cross-sectional flow area, fluid density, and pressure drop are all held constant for each case and CFD results provide the propellant mass flow rate that passes through the injection plane. Equations 1 and 2 are then applied to quantify relative hydraulic performance.

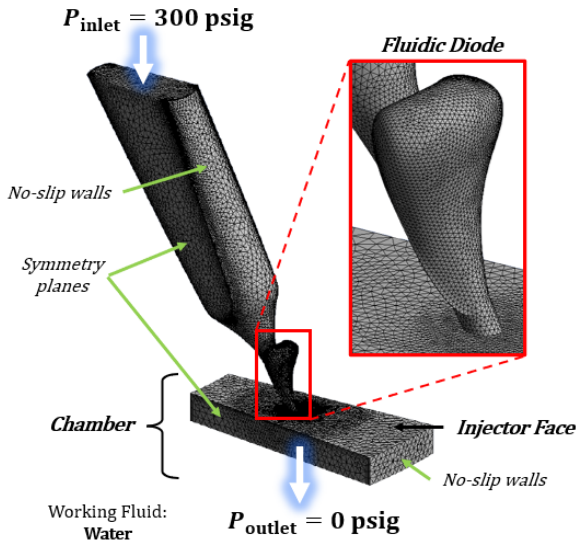

Fig. 4 Unstructured, tetrahedral mesh of a wedge-shaped symmetric slice of the chamber and the injector's fluid domain with an implemented 90° fluidic diode feature of radius R = 0.050 in. Boundary conditions shown are for the single-phase steady CFD cases.

D. Transient back-flow recovery model

A more complex CFD model was used to examine transient fluid behavior associated with a chamber pressure impulse for a smaller subset of injector designs. This model assessed the transient backflow (or flow-rate change) and interaction of liquid propellant and high pressure combustion gas within an injector element when subject to a prescribed sharp increase and decay of pressure at the injector face. Simulations were run for three different injector stiffness values: 20%, 50%, and 150%. Injector stiffness IS is defined as:

$$\mathrm{IS} \equiv \frac{\Delta p}{p_c} = \frac{p_{in} - p_c}{p_c} \tag{3}$$

The steady-state pressure drop across the injector is denoted by Δp, whereas p_c represents the steady-state chamber pressure and p_{in} is the inlet pressure.

Here, we use a pressure-based solver in ANSYS Fluent and employ an unsteady multiphase VOF (volume of fluid) model using liquid water and air as the propellant and combustion gas, respectively. Stiffness values are varied by altering the inlet pressure while the nominal chamber pressure and the peak pressure of the impulse are held constant. The transient simulation is initialized by first executing a steady case (similar to that of the steady state diodicity cases) with the initial boundary conditions used to establish nominal forward flow rates, which is what would be seen prior to applying the high-pressure impulse. Additionally, a rudimentary step-function is applied to the inlet pressure to mimic the responsive increase in manifold pressure (simulated to be an increase of ~30% relative to the initial inlet pressure) caused by gases displacing incompressible liquid propellant within the manifold. A similar manifold pressure variation is measured by researchers at Purdue in Ref. [2]. As seen in Fig. 5, a time-varying outlet boundary condition is set at t = 10 µs to mimic the pressure profile of an impulsive, high-pressure wave traversing an injector orifice and assumes the shape of an exponential decay function [2, 10, 11]. A time-step size of 1×10^{-7} seconds was found to be sufficient for a converged solution with 20 iterations per time-step. Time-step sizes smaller than this showed minimal changes in the results for the flow conditions and geometry used in this study.

IV. Results

A. Steady diodicity results

Discharge coefficients and diodicities given by the CFD simulations for the various injector designs are shown in Table 1. The diodicity of the baseline conventionally machined injector is 1.17, which was shown to increase to 1.68

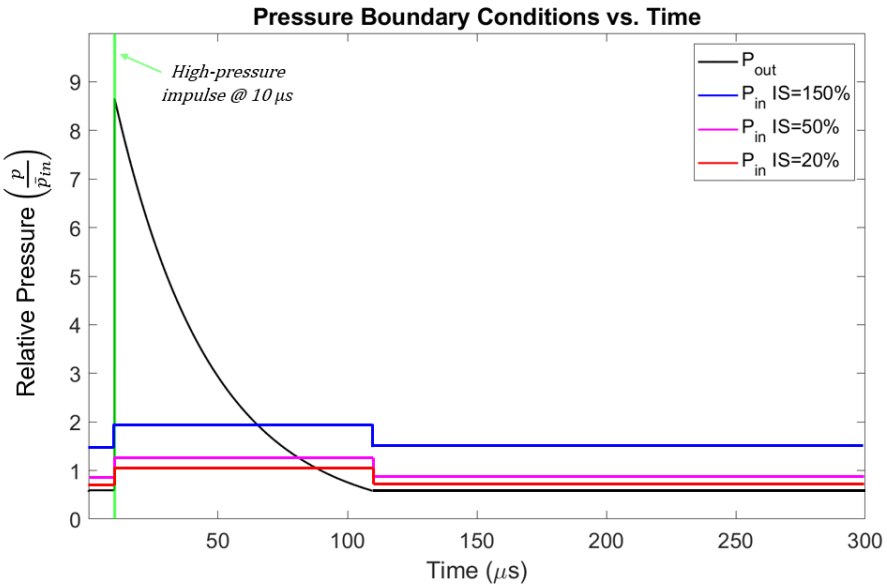

Fig. 5 Relative pressure *versus* time plots for transient boundary conditions applied to the outlet and inlet.

Injector Element Scheme	C_D Forward Flow	C_D Reverse Flow	Diodicity	Change in Diodicity relative to Baseline
Baseline	0.77	0.72	1.17	N/A
AM Tapered	0.92	0.71	1.68	+44%
90° Diode (R = 0.050")	0.92	0.54	2.90	+148%
180° Diode (R = 0.050")	0.94	0.57	2.72	+132%
360° Diode (R = 0.050")	0.94	0.56	2.82	+141%
90° Diode (R = 0.060")	0.92	0.53	3.01	+157%
Two 360° Diodes (R = 0.050")	0.90	0.52	3.00	+156%
Three 360° Diodes (R = 0.050")	0.88	0.51	2.98	+155%

Table 1 Forward and reverse discharge coefficients for the various injector element schemes as well as their corresponding diodicity values. Down-selected fluidic diode highlighted in yellow.

(+44%) for a tapered injector enabled by AM. With the introduction of various fluidic diode designs, the diodicity increases substantially to a range of 2.72 to 3.01 (upwards of +157% with respect to the baseline injector). Increasing the revolution angle of the diode resulted in increased forward and reverse discharge coefficients, but ultimately decreased the diodicity of the injector element slightly. Increasing the number of sequential diodes indicated a decrease in both forward and reverse discharge coefficients, but without a significant enhancement to diodicity. Increasing the radius of the diode 20% from 0.050" to 0.060" showed a minimal improvement to diodicity. Therefore, the 90° version of the single diode feature is chosen to be used for the transient backflow recovery simulation due to its high diodicity and its feasibility in being fabricated with AM, fulfilling wall-thickness and overhang angle requirements.

Fig. 6 shows a velocity contour plot of the fluid behavior of forward and reverse flow, and particle pathlines colored by velocity magnitude for the reverse flow case for the 90° diode feature. The fluidic diode appears to create negligible impediment to the flow in the forward direction, which yields no change in the forward discharge coefficient. On the other hand, in the reverse flow direction, fluid tends to preferentially fill the fluidic diode's reservoir and become redirected before undergoing a very sharp turn to enter the manifold inlet. This reverse flow redirection is likely responsible for the significant decline in the reverse discharge coefficient and thus an auspicious improvement in backflow resistance.

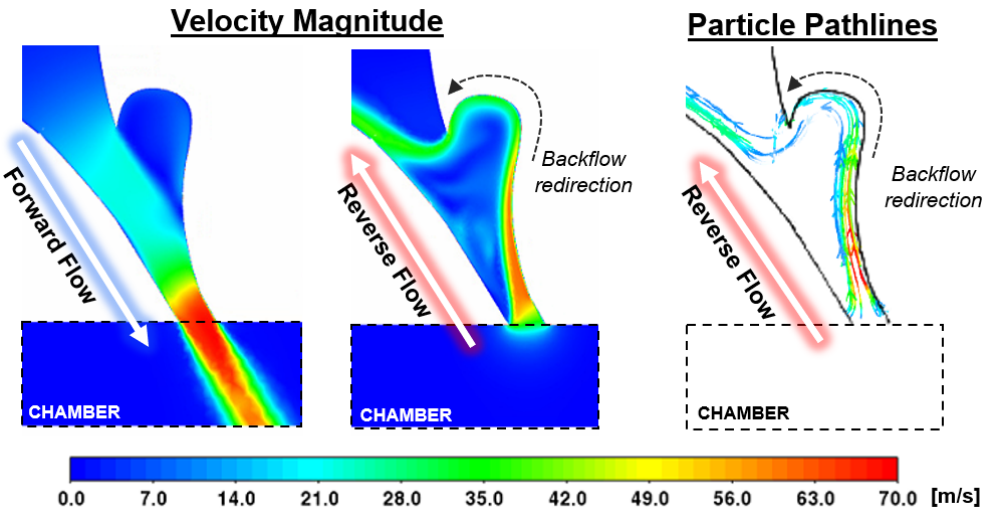

Fig. 6 Velocity contour plots of the oxidizer injector manifold with the 90° fluidic diode feature for forward flow (left) and reverse flow (middle), and particle pathlines colored by velocity magnitude for reverse flow (right).

B. Experimental validation

To date, our research group has printed and cold-flow tested some of the unlike impinging-doublet liquid bi-propellant injector designs. This includes both the baseline conventionally manufactured injector and the tapered AM injector, which was additively-manufactured using a laser powder bed fusion (L-PBF) process out of stainless steel. The tapered AM injector was cold-flow tested before and after an abrasive extrude honing process, intended to reduce surface roughness. Experimental cold-flow results are shown in Table 2 and compared to CFD results. The tapering of the internal flowpaths (even before honing) improves the forward C_D (as predicted by CFD) for both the fuel and oxidizer flow-paths relative to the baseline conventionally-manufactured injector. Moreover, significant improvement in the forward C_D is displayed after the AM injector undergoes the abrasive flow machining (honing) process. CFD results closely align with cold-flow testing for the fuel lines of both injectors, however CFD analysis seems to over-predict the forward C_D for both injectors' oxidizer lines. Despite the disagreement in absolute values, CFD was still able to accurately model the relative changes in flow behavior and thus served as a useful tool to assess relative hydraulic performance. Cold-flow results validate the hydraulic performance benefits of AM-enabled tapered flow-paths, and in conjunction with the post-printing honing process, the AM tapered injector exhibits a 21.5% and 23.4% increase in forward C_D for the fuel and oxidizer lines, respectively.

Metric	**Baseline Injector**		**AM Tapered Injector**			
	CFD	Cold Flow	CFD	Cold Flow (un-honed)	Cold Flow (honed)	% Difference after honing relative to Baseline
$C_{D,fwd,fu}$	0.80	0.79	0.91	0.87	0.96	+21.5%
$C_{D,fwd,ox}$	0.77	0.64	0.92	0.69	0.79	+23.4%

Table 2 CFD and cold-flow results showing the forward discharge coefficients of the oxidizer and fuel lines of the conventionally-machined baseline injector and the additively-manufactured tapered injector.

C. Transient backflow recovery results

Transient analysis was focused on mass flow rate changes (recovery) associated with a prescribed pressure pulse reflective of a chamber instability. Here, flow-rate recovery timescales represent figures of merit relevant to mitigating the negative effects of injector backflow on engine performance. From time-resolved mass flow rate through the injection plane, we can determine the *refill time* - the amount of time it takes from the instant of back flow occurring (when

forward mass flow rate through injector face approaches zero, denoted by t_0), until the forward flow of propellant is reestablished into the combustion chamber (when forward mass flow rate becomes positive again, denoted by t_{fwd}), as seen in Equation 4.

$$t_{\text{refill}} = t_{\text{fwd}} - t_0 \tag{4}$$

Additionally, we calculate the total amount of propellant mass vs. time by integrating the liquid mass flow rate through the injection orifice with respect to time, starting at the instant of backflow. We show the transient mass flow rate response of two injector geometries for three conditions of stiffness (reflecting a range of feed pressures) in Fig. 7a and Fig. 7b. At a high injector stiffness (i.e., 150%), the baseline and fluidic diode injector elements show a similar recovery response. However, as injector stiffness begins to decrease, the fluidic diode demonstrates a clear performance advantage as forward propellant flow rates are reestablished appreciably sooner. For injector stiffnesses of 50% and 20%, the fluidic diode permits refill times 36.8% and 39.1% sooner than the AM tapered injector, respectively.

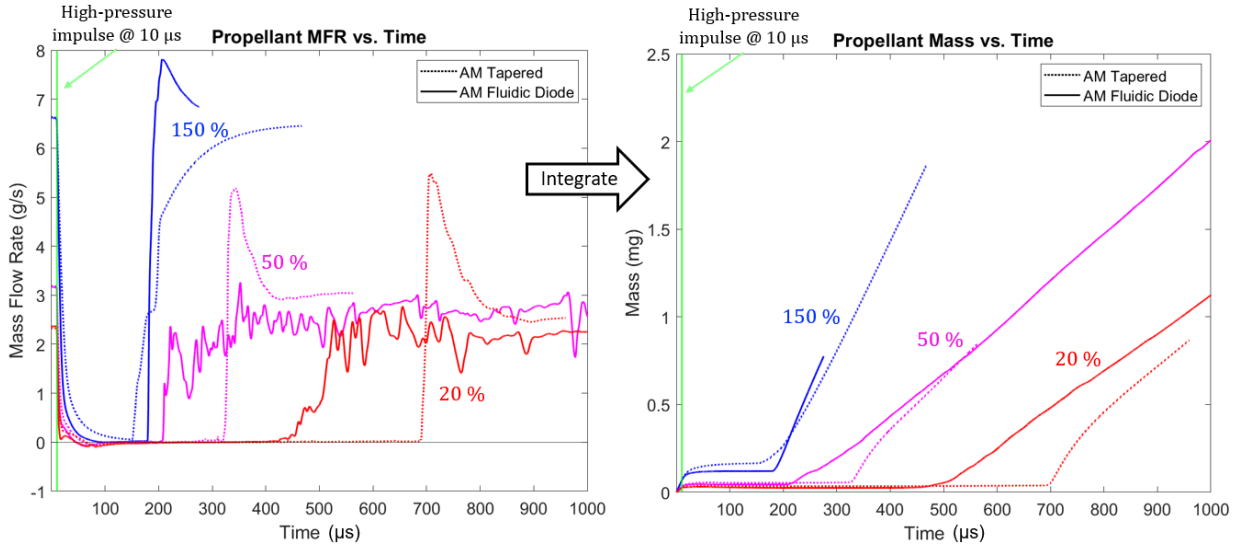

Fig. 7 (Left) Propellant mass flow rate vs. time (left), and total propellant mass vs. time (right) are plotted for three different injector stiffness values (150%, 50%, and 20%) with the AM Tapered injector geometry (dotted curves) and the AM Fluidic Diode geometry (solid curves).

Injector Stiffness	AM Tapered	AM Fluidic Diode	Difference with Fluidic Diode
150%	141 μs	169 μs	19.8% slower
50%	315 μs	199 μs	36.8% faster
20%	681 μs	415 μs	39.1% faster

Table 3 Refill times for the AM Tapered and AM Fluidic Diode injectors at three different injector stiffness values (150%, 50%, and 20%).

V. Discussion

The aforementioned combination of CFD simulations and experimental cold-flow testing reveal some key takeaways regarding potential benefits of AM-enabled non-traditional injector geometries for enhanced hydraulics and diodicity with impingement injection. Gradual tapering of traditional fluid paths is shown to offer a meaningful increase in forward discharge coefficient ($\sim$ 20%), implying lower pressure losses, which were shown to be realizable after printing

and cold-flow testing. The addition a fluidic diode feature on the tapered propellant passageways was further shown to significantly increase diodicity by as much as $\sim$ 150% compared to a conventionally-machined baseline injector case. However, the addition of multiple fluidic diodes in series exhibited marginal benefit over a single diode feature. Moreover, a fluidic diode feature that was revolved 360° around the circumference of the injector element offered no apparent benefit compared to a well-positioned 90° diode feature. This is likely associated with the impingement angle of the injector element and associated bias in inlet flow direction (entering the diode) for reverse flow. Diode feature revolution beyond 90° also presents more difficulty in reconciling feasible printing angles. Lastly, we note that based on a subset of transient cases, the diodicity determined from steady-state analysis appears to correlate with shortened flow-rate recovery times, but this is only pronounced at lower injector stiffness.

The observations mentioned above provide design insight for impingement injection with AM, but some shortcomings in the current CFD models should be noted. The models currently do not account for thermodynamics or chemical kinetics as would be associated with combustion, nor a realistic response in the manifold pressure as product gases fill the injector element. The models also do not account for surface roughness. These aspects of the model were omitted due to uncertainties, limitations in accessible computational resources and/or diminishing return on complexity. While the models lacked some sophistication, we do not expect such added elements to meaningfully alter the observed trends. It can be noted that the transient multiphase CFD model used to assess backflow recovery behavior was qualitatively validated by simulating experiments recently performed at Purdue University by Celebi et al. [2], exhibiting good agreement.

Although the constraints of additive manufacturing are fewer in comparison to conventional subtractive manufacturing techniques, they must be accounted for throughout the design process. One of the most difficult design restrictions to overcome when designing any additively-manufacturable component is staying within the overhang angle limit. This critical angle varies for different printing methods and materials, but often range between 30° to 45° with respect to the normal of the printing surface. As the injector's internal flow-path complexity increases in order to achieve desired hydraulic performance outcomes, creating a design that is printable and structurally robust becomes a more arduous task. For example, an increase in the overall size of the diode may have an increased benefit in both diodicity and recovery behavior and will be explored further in future work. However, the designer must then account for the reduction in wall-thicknesses and spacing between doublets and their adjacent element pairs by positioning the diode cavity accordingly. As such, minimal AM wall thicknesses may limit design features like element density and diode size. Some other challenges of additive manufacturing (i.e., surface roughness and sub-mm feature resolution) can be overcome by supplementing AM with post-printing processes such electrical discharge machining (EDM) and abrasive flow machining, as demonstrated [7].

VI. Summary and Future Work

This work explored the design space offered by additive manufacturing to implement geometric fluidic diode and tapering features near the injection plane for an impinging unlike doublet as a simple means of increasing diodicity. Steady single phase and transient multiphase CFD analyses demonstrate promising results: a fluidic diode feature added to a realistic injector geometry yields a favorable increase in diodicity and a quicker response time to re-establish forward propellant flow. Tapering also exhibits a decrease in forward pressure loss without meaningfully reducing backflow resistance.

At the time of this writing, a down-selected fluidic diode design has been additively manufactured and is currently in post-processing. After executing the necessary post-printing processes, this novel injector design will be similarly cold-flow tested. We have also designed and manufactured a manifold that will allow us to cold-flow injectors in the reverse direction to experimentally quantify our injectors' diodicity values under steady-state conditions.

Future computational work is aimed at evaluating the size, shape, position, and orientation of the fluidic diode features and determining their relative backflow resistance and recovery characteristics. Aside from liquid bipropellants, gas-gas and gas-liquid propellant combinations must also be investigated. Improvements are intended to the transient backflow recovery CFD model, including the ability to model the response of the manifold pressure. Additionally, the backflow recovery behavior at several other injector stiffness values (less than 20%) will be examined. This low-stiffness condition is highly applicable to mitigating liquid rocket chugg instabilities at deep throttle points.

Acknowledgments

This work was supported by the Mechanical and Aerospace Engineering Department Fellowship at UCLA, and partly supported by National Aeronautics and Space Administration (NASA), Early Stage Innovations Award No. 80NSSC20K0297. Nicolas Q. Minesi acknowledges support from NASA's Space Technology Research Grants Program (award no. 80NSSC21K0066).

References

[1] NASA, L. R. E. I., "NASA Space Vehicle Design Criteria (Chemical Propulsion)," *NASA SP-8089, March*, 1976.

[2] Celebi, H. F., Lim, D., Dille, K. J., and Heister, S. D., "Response of Angled and Tapered Liquid Injectors to Passing Detonation Fronts at High Operating Pressures," *Shock Waves*, 2021. https://doi.org/10.1007/s00193-021-01010-0, URL https://doi.org/10.1007/s00193-021-01010-0.

[3] Morrow, D., Nair, A., and Spearrin, R. M., "Minimizing hydraulic losses in additively manufactured swirl coaxial injectors," *AIAA Propulsion and Energy 2019 Forum*, American Institute of Aeronautics and Astronautics, Indianapolis, Indiana, 2019. https://doi.org/10.2514/6.2019-4310.

[4] Teasley, T. W., Protz, C. S., Larkey, A. P., Williams, B. B., and Gradl, P. R., "A Review Towards the Design Optimization of High Performance Additively Manufactured Rotating Detonation Rocket Engine Injectors," 2021, pp. 1–39. https://doi.org/10.2514/6.2021-3655.

[5] Nikola, T., "Valvular conduit," , Feb. 3 1920. US Patent 1,329,559.

[6] Thompson, S. M., Jamal, T., Paudel, B. J., and Walters, D. K., "Transitional and turbulent flow modeling in a tesla valve," *ASME International Mechanical Engineering Congress and Exposition, Proceedings (IMECE)*, Vol. 7 B, No. April 2017, 2013. https://doi.org/10.1115/IMECE2013-65526.

[7] Nair, A. P., Morrow, D., Keller, A. R., Lima, A., Pineda, D. I., and Spearrin, R. M., "Rotating Detonation of Hypergolic Space-Storable Rocket Propellants with Additively-Manufactured Injector Design," *AIAA Propulsion and Energy 2021 Forum*, American Institute of Aeronautics and Astronautics, Reston, Virginia, 2021. https://doi.org/10.2514/6.2021-3648, URL https://arc.aiaa.org/doi/10.2514/6.2021-3648.

[8] Gradl, P., Mireles, O., and Andrews, N., "Intro to Additive Manufacturing for Propulsion Systems," *AIAA Joint Propulsion Conference*, 2018.

[9] Demeneghi, G., Barnes, B., Gradl, P., Mayeur, J. R., and Hazeli, K., "Size effects on microstructure and mechanical properties of additively manufactured copper–chromium–niobium alloy," *Materials Science and Engineering A*, Vol. 820, 2021, p. 141511. https://doi.org/10.1016/j.msea.2021.141511, URL https://doi.org/10.1016/j.msea.2021.141511.

[10] Peace, J. T., Joshi, D. D., and Lu, F. K., "Experimental study of high-frequency fluidic valve injectors for detonation engine applications," *52nd Aerospace Sciences Meeting*, , No. March 2015, 2014, pp. 1–8. https://doi.org/10.2514/6.2014-1318.

[11] Lim, D., and Heister, S. D., "Transient response of a liquid injector to a transverse detonation wave at elevated initial pressure," *AIAA Aerospace Sciences Meeting, 2018*, , No. 210059, 2018. https://doi.org/10.2514/6.2018-0632.